MODELLING THE INFLUENCE OF NUCLEUS ELASTICITY ON CELL INVASION IN FIBER NETWORKS AND MICROCHANNELS

Modelling the Influence of Nucleus Elasticity on Cell Invasion in Fiber Networks and Microchannels

Marco Scianna[A,1], Luigi Preziosi[A,2]

[A] Department of Mathematical Sciences, Politecnico di Torino, Corso Duca degli Abruzzi 24, 10129 Torino, Italy

Abstract

Cell migration in highly constrained extracellular matrices is exploited in scaffold-based tissue engineering and is fundamental in a wide variety of physiological and pathological phenomena, among other in cancer invasion and development. Research into the critical processes involved in cell migration has mainly focused on cell adhesion and proteolytic degradation of the external environment. However, arising evidence has recently shown that a number of cell-derived biophysical and mechanical parameters, among others nucleus stiffness and cell deformability, plays a major role in cell motility, especially in the ameboid-like migration mode in 3D confined tissue structures. We here present an extended Cellular Potts Model (CPM) first used to simulate a microfabricated migration chip, which tests the active invasive behavior of cancer cells into narrow channels. As distinct features of our approach, cells are modeled as compartmentalized discrete objects, differentiated in the nucleus and in the cytosolic region, while the migration chamber is composed of channels of different widths. We find that cell motile phenotype and velocity in open spaces (i.e., 2D flat surfaces or large channels) is not significantly influenced by cell elastic properties. On the contrary, the migratory behavior of cells within subcellular and subnuclear structures strongly relies on the deformability of the cytosol and and the nuclear cluster, respectively. Further, we characterize two migration dynamics: a stepwise way, characterized by fluctuations in cell length, within channels smaller than nucleus dimensions and a smooth sliding (i.e., maintaining constant cell length) behavior within channels larger than the nuclear cluster. These resulting observations are then extended looking at cell migration in an artificial fiber network, which mimics cell invasion in a 3D extracellular matrix. In particular, in this case, we analyze the effect on cell movement of variations in elasticity of the nucleus. In order to summarize, with our simulated migration assays, we demonstrate that the dimensionality of the environment strongly affects the migration phenotype and we suggest that the cytoskeletal and nuclear elastic characteristics correlate with the tumor cells invasive potential.

keywords: cellular potts model · extracellular matrix · cell migration · microchannels

[1]Corresponding Author. E-Mail: marcosci1@alice.it
[2]Corresponding Author. E-Mail: luigi.preziosi@polito.it

Introduction

Cell migration on and within tissues plays a critical role in a diverse array of processes, such as in developing embryos, where the coordinated movement of cells of different origin is crucial for organogenesis and migratory defects at all stages lead to severe embryonic malformations [33]. In adult organisms, most cells are usually quiescent, except in immune surveillance or inflammation, where leukocytes actively migrate from blood vessels into infected tissues, and then into the lymph node for effector functions [15], and in wound healing, where migration contributes to the repair of both basement membrane-underlaid epithelium and connective tissues. In pathological conditions, cell migration is involved in chronic inflammatory diseases such as artheriosclerosis, and in cancer cell invasion and metastatization [54].

In particular, tumor cells are able to abandon their primary site and migrate through the surrounding parenchyma, in order to enter the circulatory system and invade other healthy tissues. On this journey, cancer individuals need to continuously regulate their migratory and invasive behavior, as they are exposed to a variety of biochemical and biomechanical interactions, modulated both by the biophysics and by the microstructure of the environment [7, 10, 31]. *In vivo* connective tissues can in fact provide interstitial extracellular matrices (ECMs) with heterogenous composition, density, and organization: they can comprise both loose regions formed by sparse collagenous fibers and areas with tightly packed threads. In the first case, important physical determinants of cell movement include the degree of ECM alignment, the width of resulting pores, and the ECM stiffness, as widely provided by experimental [8, 9, 13, 67] and theoretical [59, 68, 69] works. In the second case, matrix environments behave instead as physical barriers, adjacent to channel/track-like spaces, which, depending on their dimensionality, may either guide, hinder, or completely prevent cell movement [25, 66]. Remarkably, different studies have reported that cells achieve significant movement in highly constrained physical spaces, determined by dense matrices, by drastic morphological deformations, in addition (or even in substitution) of the proteolytical degradation of the local environment, as provided in [17, 27, 65, 66]. The repeated adaptation of cell shape requires substantial reorganization both of the cytoskeleton and of other organelles, and in particular of the nucleus, the most voluminous and rigid intracellular compartment. This type of migration, called *ameboid movement* since it is associated with flexible amoeba-like shape changes, proceeds in a poorly adhesive mode and is mostly independent from specific molecular and biochemical interactions with the surrounding system [21]. Notably, more aggressive and metastatic cancer cells have been widely shown to have a significant compliance with respect to non-metastatic individuals, which remain stuck at the vessel walls or when crossing the endothelium and therefore are forced to be confined in the primary site [21, 22, 31, 45, 51, 64].

For these reasons, a quantitative assessment of cell deformability has the potential to be of significant value for

diagnostic purposes, such as screening and cancer grading, and for a more detailed prediction of the course of the disease in individual patients [55]: indeed, it has given rise to a number of *in vitro* models. For instance, 3D lattices consisting of reconstituted fibrillar collagen are typically used to study cell migration in structures mimicking highly confined *in vivo* connective tissues [67]. However, in most cases, these bio-engineered scaffolds lack well-controlled spatial characteristics, because small and large pores results from the stochastic fiber polymerization processes, therefore failing to recreate defined trails and barriers [8, 50, 67]. Indeed, specific mechanisms of reassembly of fibrillar matrices have been recently combined with microlaser procedures, able to generate predefined tracks that create spatially defined patterns of connective tissue organizations [27]. At this regard, geometrical characteristics of 3D matrix environments can be easily controlled and modulated also with migration assays whose key features are micro-sized channel structures [28, 53].

Such different types of experimental systems are here reproduced and simulated by an extended cellular Potts model (CPM, [2, 18, 19, 20, 40, 58]). It is a grid-based Monte Carlo technique which employs a stochastic energy minimization principle to display the invasiveness of tumor cells into well-defined and controlled 3D environments. As distinct features of the proposed approach, each cell is modeled as a discrete physical unit, compartmentalized into the nucleus and the cytosol, and characteristics like cell morphological evolutions and directionality are not imposed *a priori*, but are the result of their interactions with the extracellular environment.

The method is used to extract the main features of tumor cell invasiveness by working first with a 3D channel environment. As an outcome, we focus on experimentally addressable characteristics of cell locomotion, i.e. overall displacement and velocity, predicting how these quantities are influenced by manipulations either of the geometrical features of the channels, or of the biophysical properties (i.e., elasticity) of the cells themselves. We then use the simulated migration chip to compare the migration of cells inside the microchannels and their movement on a 2D flat surface, like the one located before the entrance of the channels. Consistently with experimental observations on different tumor cell lines, our approach allows to discern the effect of the mechanical rigidity of each cell compartment (i.e., the nucleus and the cytosolic region) in the migration capacity of the entire individual. Moreover, our findings provide evidence of the facts that migration characteristics of cells are very different in 2D and in highly constrained 3D environments and that even the underlying dynamics change.

The same approach is finally employed to focus on cell migration in regular networks of fibres, which mimic extracellular matrices (ECM) with different densities (i.e., with different pore dimensions). Also in this case, we analyze the permissive role played in cell locomotion of the nucleus elasticity.

The remaining parts of this publication are organized as follows: in Section 2 (Mathematical Model), we clarify the assumptions on which our approach is based. The computational findings are then presented in Section 3 (Results),

where we separate the microchannel-based simulations from the realizations of cell movement in fibrous scaffolds. Finally, the results are discussed in Section 4 (Discussion).

Mathematical Model

The microchannel device and the fibrous scaffold are modeled at the mesoscopic level using an extended Cellular Potts Model, a grid-based stochastic approach, which realistically preserves the identity of the single cancer cells and describes their behavior and interactions with the local microenvironment in energetic terms and constraints. The simulation domains are three-dimensional regular lattices $\Omega \subset \mathbb{R}^3$, formed by identical closed grid sites that, with an abuse of notation, will be identified by their center $\mathbf{x} \in \mathbb{R}^3$. Each grid site is labeled by an integer number, $\sigma(\mathbf{x}) \in \mathbb{N}$, that can be interpreted as a degenerate *spin* originally coming from the statistical physics [30, 48]. The border of a lattice site $\mathbf{x}$ is identified as $\partial\mathbf{x}$, one of its neighbors by $\mathbf{x}'$, while its overall neighborhood by $\Omega^{'}_{\mathbf{x}}$, i.e. $\Omega^{'}_{\mathbf{x}} = \{\mathbf{x}' \in \Omega : \mathbf{x}' \text{ is a neighbor of } \mathbf{x}\}$. Subdomains of contiguous sites with identical spin form discrete objects Σ_σ (i.e., $\Sigma_{\overline{\sigma}} = \{\mathbf{x} \in \Omega : \sigma(\mathbf{x}) = \overline{\sigma}\}$) which have an associated type $\tau(\Sigma_\sigma)$.

The simulated cancer cells, called η, are defined as compartmentalized units, composed of two subregions which, in turn, are classical CPM objects Σ_σ: the nucleus, a central cluster of type $\tau = N$, and the surrounding cytosol, of type $\tau = C$. Each cell compartment is obviously characterized, as an additional attribute, by the cluster id η to identify the individual it belongs to. The extracellular environments, i.e. the microchannel chip and the fibrous scaffold, are differentiated in a medium-like state, $\tau = M$, and a polymeric-like state, $\tau = P$. The medium-like state represents the mixture of soluble components, which, together with the water solvent, compose the interstitial fluid. It is assumed to be isotropically distributed throughout the simulation domain, forming no large-scale structures. The polymeric state reproduces instead either the structured wafer, which, after subsequent replica molding processes, is typically covered with fibronectin-based solutions and used in the standard micro-fabricated channel migration chip, see [53] and references therein, or the ECM fiber network.

The simulated experimental system evolves to iteratively and stochastically reduce its free energy, defined by the *hamiltonian* H, whose expression will be clarified below. The core algorithm is a modified Metropolis method for Monte Carlo-Boltzmann dynamics [20, 43], which is able to implement the natural exploratory behavior of biological individuals. Procedurally, at each time step t, called Monte Carlo Step (MCS, the basic unit of time of the model), a lattice site belonging to a cell compartment Σ_σ, $\mathbf{x}_{source}$, is selected at random and assigns its spin, $\sigma(\mathbf{x}_{source})$, to one of its unlike neighbors, $\mathbf{x}_{target} \in \Omega^{'}_{\mathbf{x}_{source}} : \mathbf{x}_{target} \notin \Sigma_\sigma$, also randomly selected. The net energy difference due to the proposed change of domain configuration, $\Delta H|_{\sigma(\mathbf{x}_{source})\to\sigma(\mathbf{x}_{target})} = H_{(after\ spin\ copy)} - H_{(before\ spin\ copy)}$, is

then evaluated. The trial spin update is finally accepted with a Boltzmann-like probability function:

$$P(\sigma(\mathbf{x}_{source}) \to \sigma(\mathbf{x}'_{target}))(t) = \tanh(\varepsilon T_{\Sigma_{\sigma(\mathbf{x}_{source})}}(t)) \min\{1, e^{-\Delta H/T_{\Sigma_{\sigma(\mathbf{x}_{source})}}(t)}\}, \tag{1}$$

where $T_{\Sigma_{\sigma(\mathbf{x}_{source})}}(t) \in \mathbb{R}_+$ is a Boltzmann temperature that measures the agitation rate of moving object $\Sigma_{\sigma(\mathbf{x}_{source})}$. The specific form of (1) is a modification of the standard Boltzmann probability function, used in classical CPM applications and recovered in the limit $\varepsilon \to \infty$. As commented in [58], the classical law has a significant weakness in the fact that, for non positive energy gradients, each object Σ_σ is going to move, regardless of its intrinsic motility, defined by T_{Σ_σ}. This lacks of biological realism: for example a frozen individual, pretreated by cytochalasin B or held at 4 °C, has a null probability to move in all situations. In order to address this issue (i.e., to take into account the cell agitation rate also in the case of energetically unfavorable displacement attempts), in [58] it was then proposed to multiply the standard Boltzmann law by a sort of *maximal transition probability* function, which depends on T_{Σ_σ} and, in particular, is zero for T_{Σ_σ}=0 and goes to one in the case of high values of T_{Σ_σ}. Indeed, for $\tau(\Sigma_{\sigma(\mathbf{x}_{source})}) = N$, $T_{\Sigma_{\sigma(\mathbf{x}_{source})}} = T_N$ gives the agitation rate of cell nucleus, while, for $\tau(\Sigma_{\sigma(\mathbf{x}_{source})}) = C$, $T_{\Sigma_{\sigma(\mathbf{x}_{source})}} = T_C$ is a measure of the intrinsic motility of the overall individual, as it gives the frequency of the ruffles of its cytosol (which, on a molecular level, are determined by polarization/depolarization processes of the actin cytoskeleton, refer to [44, 47, 52] and references therein). For each cell η, T_N is a low value, resulting in the passive motion of the nucleus, which, unable to have an autonomous movement, is dragged by the surrounding cytosol, characterized instead by a high T_C (see [57] for a more detailed mechanical explanation). Obviously, the extracellular structure (both the channel architecture and the fiber mesh) is fixed.

For any given time t, the system *hamiltonian*, whose minimization drives the evolution of the system, is defined as:

$$H(t) = H_{shape}(t) + H_{adhesion}(t) + H_{persistence}(t). \tag{2}$$

For each cell η, H_{shape} models the geometrical attributes of its subcellular compartments, which are written as non-dimensional relative deformations in the following quadratic form:

$$H_{shape}(t) = H_{volume}(t) + H_{surface}(t) = \sum_{\Sigma_\sigma} \left[\kappa_{\Sigma_\sigma}(t) \left(\frac{v_{\Sigma_\sigma}(t) - V_{\tau(\Sigma_\sigma)}}{v_{\Sigma_\sigma}(t)} \right)^2 + \nu_{\Sigma_\sigma}(t) \left(\frac{s_{\Sigma_\sigma}(t) - S_{\tau(\Sigma_\sigma)}}{s_{\Sigma_\sigma}(t)} \right)^2 \right], \tag{3}$$

depending on the actual volume and surface of the subcellular units, $v_{\Sigma_\sigma}(t)$ and $s_{\Sigma_\sigma}(t)$, as well as on the same quantities in the relaxed state, $V_{\tau(\Sigma_\sigma)}$ and $S_{\tau(\Sigma_\sigma)}$, which correspond to their initial measures. The formulation of (3) presents a blow up in the case of $v_{\Sigma_\sigma}(t), s_{\Sigma_\sigma}(t) \to 0$, meaning that for instance an infinite energy would be required

to shrink a cell to a point, see again [58] for a detailed explanation. $\kappa_{\Sigma_\sigma}(t)$ and $\nu_{\Sigma_\sigma}(t) \in \mathbb{R}^+$ are mechanical moduli in units of energy: in particular, $\kappa_{\Sigma_\sigma}(t)$ refer to volume changes, while $\nu_{\Sigma_\sigma}(t)$ relates to the deformability/elasticity of the related subcellular compartment, i.e. the ease with which it is able to remodel. Assuming that cells do not significantly grow during migration (which is consistent with the time-scale of the phenomenon of our interest), the fluctuations of their volumes are kept negligible with high constant values $\kappa_{\Sigma_\sigma} = \kappa \gg 1$, for any individual η and for Σ_σ such that $\tau(\Sigma_\sigma) = \{N, C\}$. The stiffness of the intracellular compartments (given, respectively, by $\nu_{\Sigma_\sigma} = \nu_C$, for $\tau(\Sigma_\sigma) = C$ and $\nu_{\Sigma_\sigma} = \nu_N$, for $\tau(\Sigma_\sigma) = N$) will be instead discussed in the result section.

$H_{adhesion}$ is the general extension of Steinberg's Differential Adhesion Hypothesis (DAH) [20, 60, 61]. In particular, it is differentiated in the contributions due to either the generalized contact tension between the nucleus and the cytoplasm within the same cell, or to the effective adhesion between cells or between a cell and an extracellular component:

$$\begin{aligned} H_{adhesion}(t) &= H^{int}_{adhesion}(t) + H^{ext}_{adhesion}(t) = \\ &= \sum_{\substack{(\partial\mathbf{x}\in\partial\Sigma_\sigma)\cap(\partial\mathbf{x}'\in\partial\Sigma_{\sigma'}) \\ \eta(\Sigma_{\sigma(\mathbf{x})})=\eta(\Sigma_{\sigma(\mathbf{x}')})}} J^{int}_{\tau(\Sigma_{\sigma(\mathbf{x})}),\tau(\Sigma_{\sigma(\mathbf{x}')})} + \sum_{\substack{(\partial\mathbf{x}\in\partial\Sigma_\sigma)\cap(\partial\mathbf{x}'\in\partial\Sigma_{\sigma'}) \\ \eta(\Sigma_{\sigma(\mathbf{x})})\neq\eta(\Sigma_{\sigma(\mathbf{x}')})}} J^{ext}_{\tau(\Sigma_{\sigma(\mathbf{x})}),\tau(\Sigma_{\sigma(\mathbf{x}')})}, \end{aligned} \tag{4}$$

where $\mathbf{x}$ and $\mathbf{x}'$ are two neighboring sites (i.e., $\mathbf{x}' \in \Omega'_{\mathbf{x}}$) and $\Sigma_{\sigma(\mathbf{x})}$ and $\Sigma_{\sigma(\mathbf{x}')}$ two neighboring objects. The coefficients $J_{\tau(\Sigma_\sigma),\tau(\Sigma_{\sigma'})} \in \mathbb{R}$ are binding forces per unit area, and are obviously symmetric w.r.t. the indices. In particular, $J^{int}_{N,C}$ implicitly models the forces exerted by intermediate actin filaments and microtubules to anchor the nucleus to the cell cytoskeleton, preventing cells from fragmenting, while $J^{ext}_{C,C}$ represents the local adhesive strength between neighbouring cells, a measure of the local quantity of active and exposed cadherin molecules. $J^{ext}_{C,M}$ and $J^{ext}_{C,P}$ evaluate instead the heterophilic contact interactions between a cell and an extracellular component. On one hand, $J^{ext}_{C,M}$ accounts for the adhesiveness between the cell membrane and specific soluble ligands present in the medium. On the other hand, $J^{ext}_{C,P}$ measures the affinity between integrins complexes on the cell surface and either the fibronectin gel covering the solid structure of the microchannel device or the matrix threads forming the fibrous scaffold. In particular, given $J^{int}_{N,C} \ll 0$ to prevent cell splitting, we give null contribution to the adhesive interactions between a moving cell and an extracellular component (i.e., we assume $J^{ext}_{C,M} = J^{ext}_{C,P} = 0$). This choice, successfully used in another similar model of *in vitro* cell migration [57], is done to analyze the direct influence of cell deformability on its motile behavior, and is consistent with experimental literature, which widely demonstrates that most cell lines display sustained ameboid motility in confined environments in a poorly adhesive mode [21, 34, 53]. $J^{ext}_{C,C}$ is finally kept high to avoid cell-cell adhesive interactions that may affect the early phases of their movement (i.e., on the flat

surface outside the channels). By setting constant and homogeneous values for the bond energies Js, we here assume a uniform distribution of adhesion molecules both on cell surfaces and in the external environment, without any change during the observation time.

Finally, if moving cells are able to polarize, i.e. to differentiate in a leading and a trailing surface, they display a directional movement dictated by their longer axis. For each individual η, this inertial, shape-dependent motion is modeled with a further energy term, which is coherently a running mean over the cell past movements [2, 56]:

$$H_{persistence} = \mu^{\eta}_{pers}(t)||\mathbf{v}_{\eta}(t) - \mathbf{v}_{\eta}(t - \Delta t)||^2, \tag{5}$$

where $\mathbf{v}_{\eta}(t)$ is the instantaneous velocity of the cell center of mass. μ^{η}_{pers} controls the persistence time of cell η and is:

$$\mu^{\eta}_{pers}(t) = \mu_{pers,0}\left[\frac{L_{\eta}(t)}{L_0} - 1\right], \tag{6}$$

L_{η} is the current length of the longer axis of the cell, which is approximated with an ellipsoid [41], and L_0 is the initial cell diameter. Obviously $L_{\eta} \geq L_0$, since we have assumed that the cell deforms but does not grow during migration. Eq. (6) is based on the experimental evidence provided in [26], where in similar conditions elongated vascular cells have seen to have a longer persistence time than more rounded cells. This is explained with the observation that cell polarization is a cytoskeleton-driven process: the more a cell is polarized (i.e., the longer its main axes is), the more its actin filaments are in fact oriented in such a direction, requiring a longer time to reorient into a new direction, and thus to change the direction of motion of the whole cell. Coherently, from (6), if $\mu^{\eta}_{pers} = 0$ the cell undergoes uncorrelated Brownian motion, while if μ^{η}_{pers} is very large its motion is almost ballistic.

A summary of the parameters used in the model is given in Table 1. In particular, the estimated values have been accurately inferred on the basis of experimental observations, which are specified along the text. At this regard, we have observed that the behavior of the model is fairly robust in sufficiently large regions of parameter space around our estimates.

Table 1: Summary of the parameters used in the model. $(*)$ indicates those that vary in the different sets of simulations

Parameter	Description	Value	Reference(s)
V_N	volume of cell nucleus	523 [μm^3]	[4, 53]
S_N	surface of cell nucleus	314 [μm^2]	[4, 53]
V_C	volume of cell cytosol	6542 [μm^3]	[4, 53]
S_C	surface of cell cytosol	3140 [μm^2]	[4, 53]
ε	coefficient of Boltzmann-like probability function	1	[58]
T_N	motility of cell nucleus	0.25	[57]
T_C	motility of cell cytosol	9	estimated
κ	compressibility of cell volume	15	estimated
ν_C	rigidity of cell cytosol	15 ; 0.5*	estimated
ν_N	rigidity of cell nucleus	15 ; 0.9*	estimated
$J^{int}_{N,C}$	generalized adhesion between nucleus and cytosol	-20	[57, 58]
$J^{ext}_{C,C}$	cell-cell adhesive strength	20	estimated
$J^{ext}_{C,M}$	cell-medium adhesive strength	0	[57]
$J^{ext}_{C,P}$	cell-fibronectin gel/cell-fiber adhesive strength	0	[57]
$\mu_{pers,0}$	basal persistence strength	0.8	estimated

Simulation Characteristics and Results

Migration in a Microchannel Structure

The simulation domain $\Omega \subset \mathbb{R}^3$ is a 480 $\times$ 288 $\times$ 48 regular grid, with periodic boundary conditions in the y direction and no flux in the others. The characteristic size of each grid site is 1 μm. The lattice reproduces a micro-fabricated device with channel structures of various widths and a planar surface just outside their entrances, see Fig. 1. This architecture is typically used in literature to analyze cell migration both on open spaces and through precisely confined environments, see [53] and references therein. The temporal resolution of the model is a MCS, which is set to correspond to 2 s in order to compare the simulated cellular dynamics with the relative experimental observations. The overall observation time is set equal to 8 hours ($\approx$ 14400 MCS) to ensure the development of sufficiently long migration paths, as done again in [53]. Initially, the cells are seeded on the planar substrate in the close proximity to the channel entrances and display an unpolarized morphology. Indeed, they are hemispheres 30 μm long and wide and 15 μm high, while the nucleus, whose location and geometry is estimated from experimental images, is a central sphere with a diameter of 10 μm. These dimensions, given in Table 1, reflect the mean measures of human pancreatic epithelial cancer cells (Panc-1) [4, 53].

Following the definition used in [53], we here distinguish cell migratory behavior as follows:

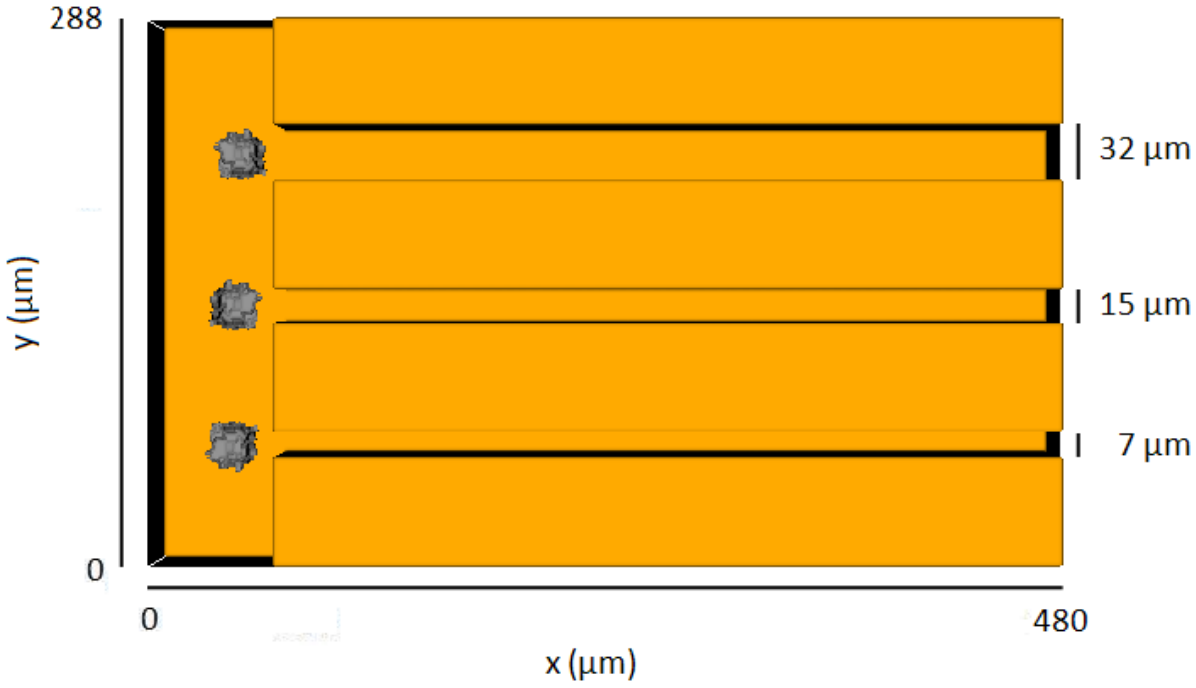

bottom channel size < nucleus diameter < middle channel size < cell diameter < top channel size

Figure 1: Sections of the simulation domain Ω. The lattice, characterized by periodic boundary conditions in the y direction and no flux in the others, reproduces a micro-fabricated device with channels of various width and a planar surface just outside their entrance. In particular, the top channel is larger than the overall cell diameter, while the bottom channel is smaller than nuclear dimensions. Initially, the cells are seeded on the flat substrate near the channel walls.

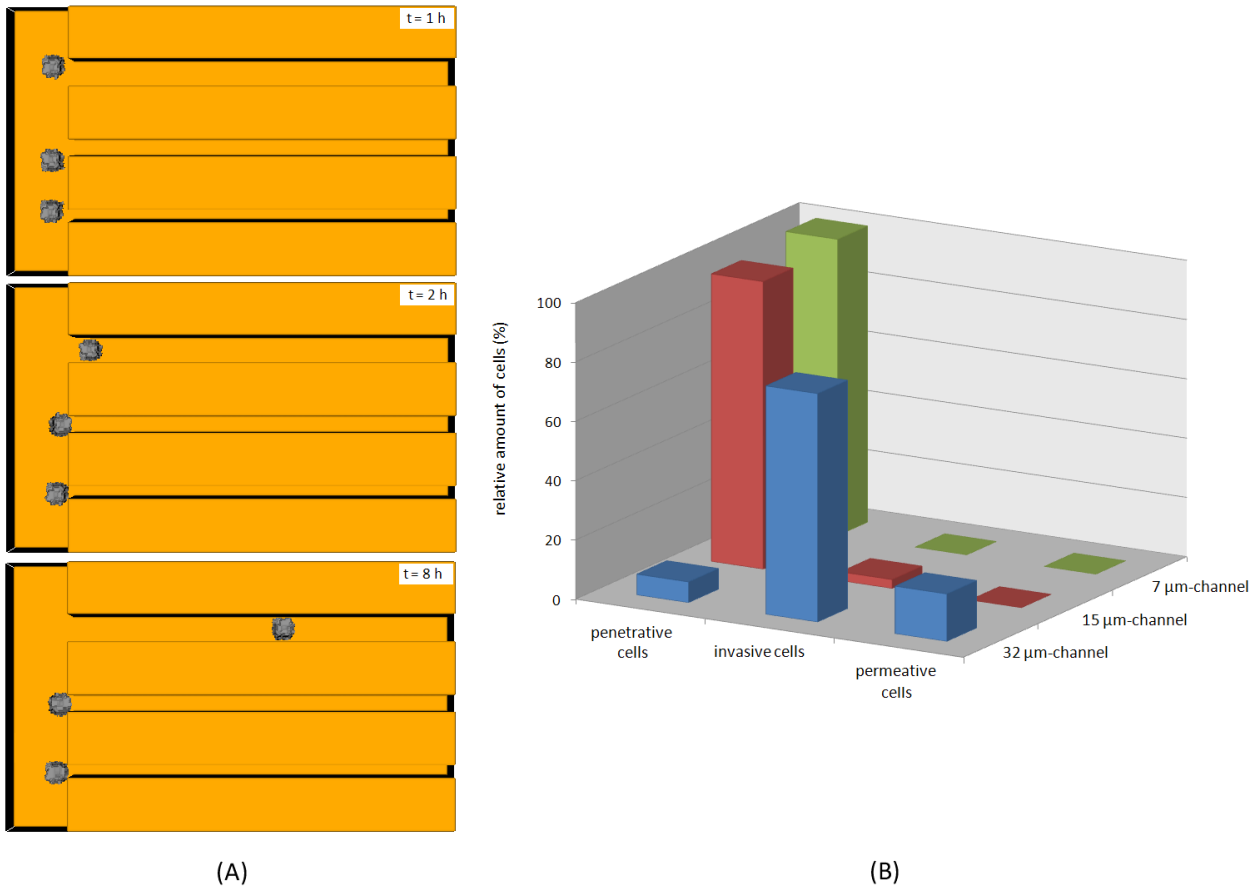

Figure 2: Migratory behavior within the microchannel structure of cancer cells unable to remodel at all (i.e., characterized by a high $\nu_{\Sigma_\sigma} = 15$, for $\tau(\Sigma_\sigma) = \{C, N\}$). (A) Images of a time-lapse simulation taken at t= 1 (top panel), 2 (middle panel), and 8 (bottom panel) hours. Only the largest channel can be entered by moving individuals, which, forced to remain in their initial hemispheric morphology, are prohibited to squeezed through smaller structures. (B) Summary of cell migratory behavior within the matrix device. In the case of middle and small channels, cells display a penetrative non-invasive phenotype, whereas in the case of the biggest channel, they are typically invasive. The quantitative evaluation of specific cell motile phenotypes, represented in the histogram plot, is obtained by performing 100 simulations.

- cells that only penetrate a channel with a part of their cytoplasm but not with the nucleus are classified as *penetrating*,
- cells that completely enter a channel structure but are not able to migrate to the other side within the observation period are called *invasive*,
- cells that reach the opposite border of a channel are finally termed *permeative*.

The motile phenotypes are also characterized in our analysis by:

- the so-called *entry time*, defined as the time span from the first contact of a cell with a channel to the moment when the whole cell body is completely inside it [37]. This parameter therefore quantifies the time needed by

an individual to deform and invade the structure of interest;

- the *deformation* of a cell (respectively, of its nucleus), defined as the ratio between the surface of the cell (respectively, of its nucleus) at the end of the migration and its initial value. Given that the cell volume (respectively, the nucleus volume) is kept nearly fixed by high values of κ, this quantity gives a specific measure of cell (respectively, nucleus) shape reorganization.

In the first set of simulations, we force cancer cells to maintain their hemispherical shape by setting high $\nu_N = \nu_C = 15$. This is the model counterpart of the activity of phalloidin-like compounds, which block the reorganization of the cell cytoskeleton by inhibiting actin-myosin interactions. As reproduced in Fig. 2, all individuals initially show a random migration on the flat surface (i.e., until nearly 2 hours). Then, when approaching the channel walls, they start walking along them. At this regard, it is useful to underline that this preferred cell movement is completely autonomous, as we do not include in the model any chemical gradient or bias, or any *a priori* direction for moving individuals. In the case of the channel with the largest cross-section, the cells typically display an invasive behavior, as they are able to quickly enter and migrate within the structure (i.e., the characteristic entry time is low, see the top plot in Fig. 5), but not to reach the opposite border, as shown in Fig. 2. Migrating individuals in fact fluctuate and "rebound" between channel internal walls, whose width does not represent a significant geometrical *contact guidance*. Indeed, cells do not reach an appreciable directional velocity, remaining almost in the middle of the structure. Cell migration both in the middle and in the small channel (whose widths are smaller than cellular dimensions) is instead characterized by a penetrative phenotype. Without the possibility to deform in a substantial way, the individuals are in fact prohibited to squeeze through the confined environments. Therefore, they continue to isotropically wonder in the close proximity of the channel entrances.

We then analyze how the motile behavior of cells is affected by the remodeling of their cytoskeleton. Indeed, the elasticity of the cell cytosolic region is allowed by a lower value of $\nu_C = 0.5$, whereas the nuclear cluster is maintained rigid by the same high value for ν_N ($= 15$). With respect to the previous set of simulations, the initial non-directed movement of cells on the planar substrate is accompanied by a non-negligible spreading (see Fig. 5(bottom right plot)). As reproduced in Figs. 3 and 5(top plot), the cell migratory behavior in the largest channel, as well as the characteristic entry time, remains unaltered, regardless of cytosolic deformation abilities. As already observed, moving individuals in fact do not experience significative steric hindrances that require substantial morphological changes (see again Fig. 5(bottom right plot)) and almost display the same invasive phenotype. At the intermediate channel width (i.e., smaller than cellular dimensions and bigger than nuclear dimensions), cells with a deformable cytoplasm are instead able to squeeze into and move within the microstructure, as captured by the bottom right graph in Fig. 5. In particular,

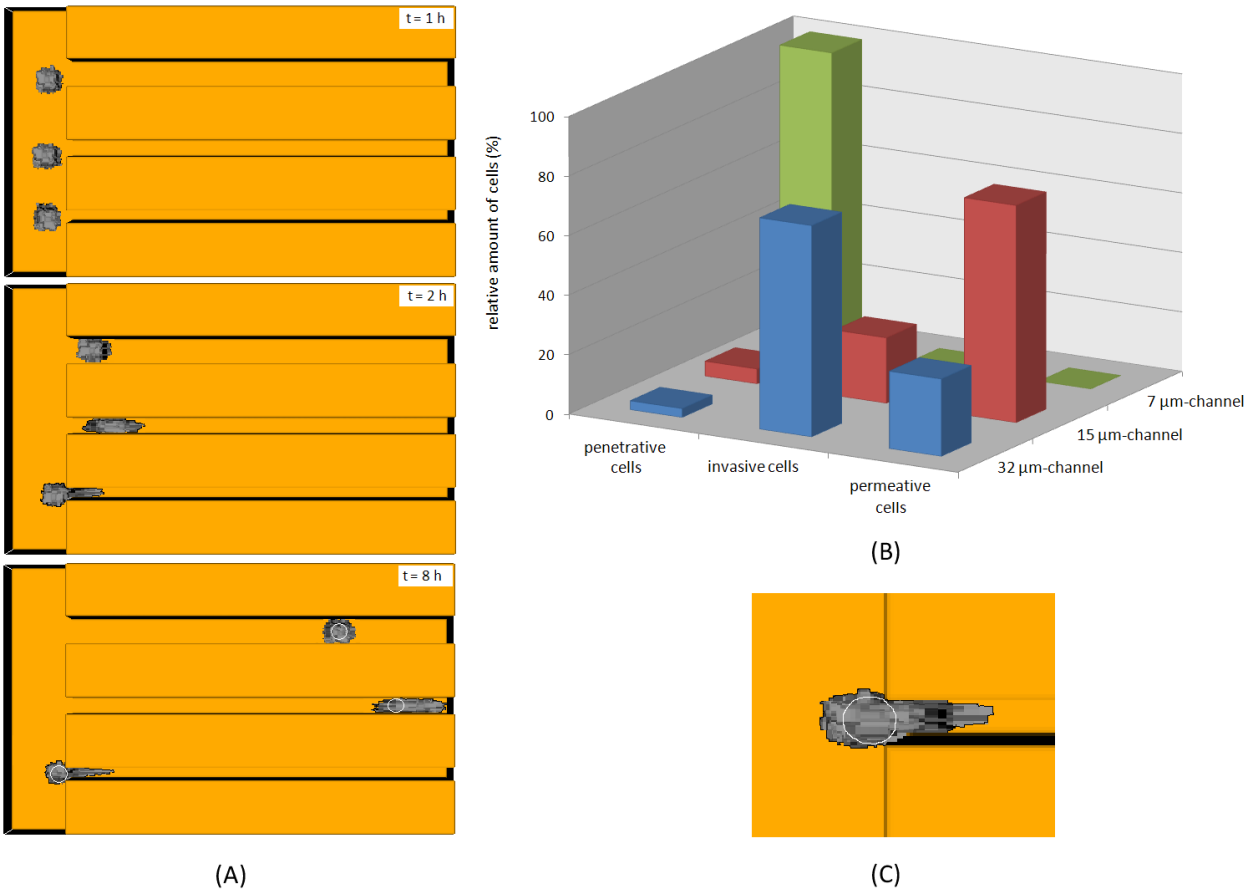

Figure 3: Migratory behavior within the microchannel structure of cancer cells with an elastic cytosol and a still rigid nucleus (i.e., $\nu_C \ll \nu_N$). (A) Images of a time-lapse simulation taken at t= 1 (top panel), 2 (middle panel), and 8 (bottom panel) hours. By dramatically remodeling their cytoskeleton, cells are now able to enter also in the intermediate channel. However, due to the presence of a stiff nucleus, they can not penetrate into the smallest structure. For better visualization, in the bottom panel, the nucleus is encircled manually. (B) Summary of cell migratory behavior within the matrix device. In the case of the widest channel, cells display the same invasive behavior as in Fig. 2. In the case of the middle channels, they instead acquire a permeative phenotype. Finally, in the smallest channel, cells are still penetrative but un-invasive. The quantitative evaluation of specific cell motile phenotypes, represented in the histogram plot, is obtained by performing 100 simulations. (C) Magnification of moving cell in the close proximity of the smallest channel entrance. It is straightforward to see how the stiff voluminous nucleus is not able to pass through the confined space, allowing only the penetration of part of the cytosol.

they remodel towards an elongated shape and typically migrate to the other end of the device, displaying a common permeative phenotype, see again Fig. 3. The transition from a stationary cell morphology to a polarized shape, which is completely self generating and due to the geometry of the matrix environment, is fundamental in determining the persistent component in cell movement. With a modeling view point, cell elongation in fact increases the relative magnitude of the persistence term (5) in the overall hamiltonian, given by coefficient μ^{η}_{pers}. Therefore, once a cell has established the direction of movement within a channel, it is energetically disadvantageous to change direction and is forced to maintain the direction of locomotion. Finally, cells are still not able to enter the smallest channel. If the front

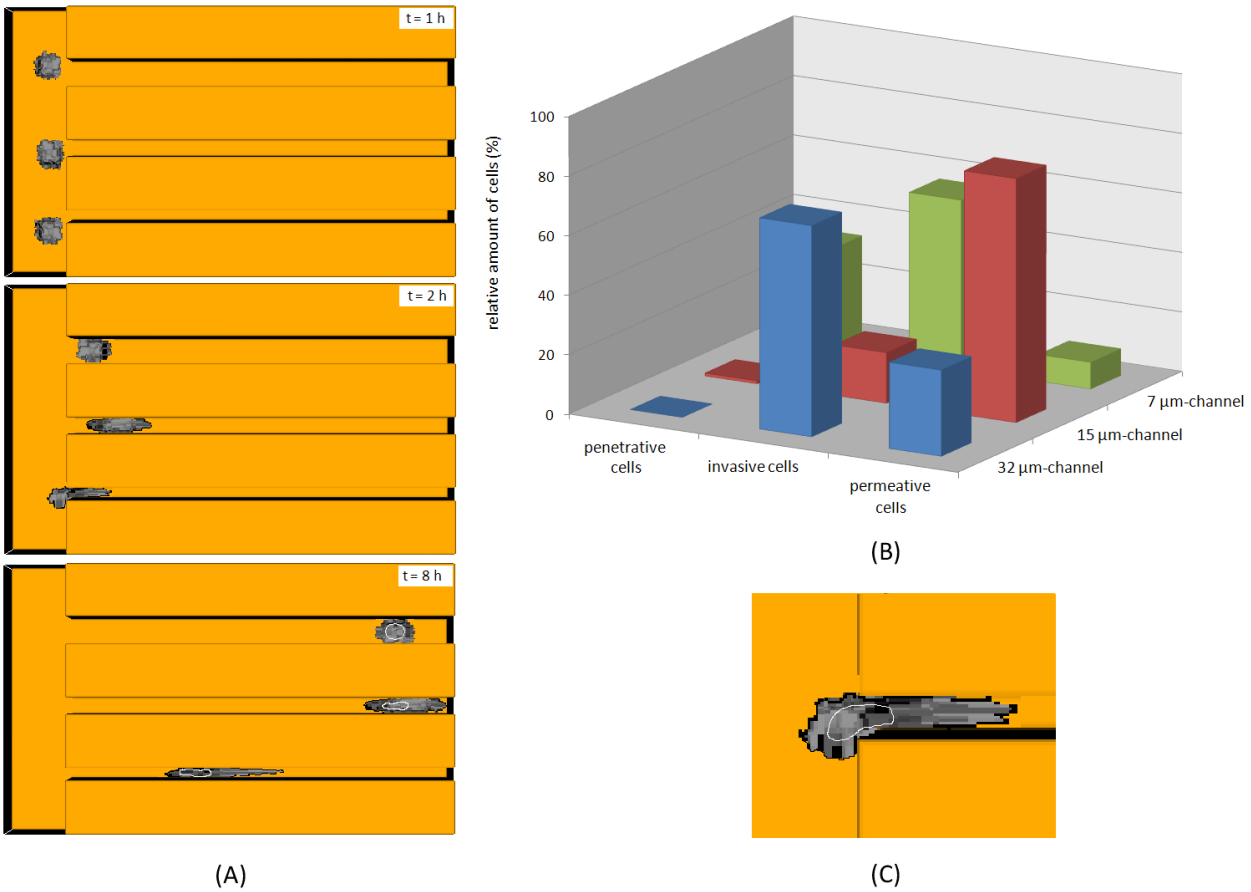

Figure 4: Migratory behavior within the microchannel structure of cells with an elastic cytosol and a deformable nucleus (i.e., $\nu_N = 0.9$). (A) Images of a time-lapse simulation taken at t= 1 (top panel), 2 (middle panel), and 8 (bottom panel) hours. The enhancement in nucleus elasticity enables cells to enter also in the smallest channel. For better visualization, in the bottom panel, the nucleus is encircled manually. (B) Summary of cell migratory behavior within the matrix device. In the case of the widest channel, cells display the same invasive behavior as in Fig. 2. In the case of the middle channels, the permeative phenotype is enforced. Finally, in the smaller channel, cells acquire an invasive ability. The quantitative evaluation of specific cell motile phenotypes, represented in the histogram plot, is obtained by performing 100 simulations. (C) Magnification of moving cell in the close proximity of the smaller channel entrance. It is straightforward to see how the nucleus can now squeeze to pass within the channel entrance, allowing the entire individual to invade the structure.

of their cytoplasm quickly extends into the structure, the voluminous nuclear region can not in fact deform and pass through such a highly constrained space, therefore inhibiting the individual to pull inside its entire body, as clearly reproduced in Fig. 3(C).

Our results are consistent with the experimental observations provided in [4], where the authors used a Boyden chamber assay to correlate an increment in the ability of pancreatic cancer cells (Panc-1) to squeeze and migrate through microporous membranes to a drop in their elastic modulus, measured by a micro-plate based single-cell stretcher.

We next address the question to what extent a variation in cell nucleus elasticity enables cell invasion and movement into highly confined spaces. If in the model the rigidity of nucleus is determined by the value of parameter ν_N, biologically it is mainly regulated by:

- the chromatin structure, a combination of DNA and proteins (primarily histones) that makes up the contents of the nucleus [5, 39];
- the network of intermediate filaments, which is constituted, among others, by lamin proteins and keratin molecules and which has a fundamental structural function. In particular, the lamins localize in the nuclear lamina (a proteinaceous structure layer subjacent to the inner surface of the nuclear envelope) and throughout the nucleoplasm (in the so-called nucleoplasmic "veil") [14, 17]. The keratins are instead generally found in the cytoplasm, however, upon external induction they are able to reorganize in the perinuclear region, thereby increasing the mobility and the elasticity of the nucleus itself [38].

The decrement of ν_N, fixed equal to 0.9, can therefore model a modification of the chromatin structure, a remodeling of lamin filaments or an experimental treatment with micromolar concentrations of bioactive lipid sphingosylphosphorylcholine (SPC), whose activity leads to a substantial translocation of the keratin network towards a perinuclear rearrangement [4, 62]. However, we opt to maintain $\nu_N > \nu_C$, since the cytoplasmic region of the cell remains typically softer than the even more elastic nuclear cluster.

The analysis of the model outcomes, summarized in Fig. 4, reveals that, in the case of the largest channel, the deformability of the nucleus does not appreciably affect cell migratory behavior. When the channel dimension decreases to the intermediate range, though the cell morphology looks almost similar to the previous case, the nuclear elasticity provides a further facilitation for the movement of the entire individual. In fact, the number of permeative cells increases. This is due both to the fact that moving cells can now more easily and more quickly pass through the channel entrance (the entry time significantly decreases, see Fig. 5) and to the fact that they can more efficiently migrate within its walls, as also their voluminous nuclear region is able to assume a more elongated and "mobile" configuration, allowing a more efficient deformation of the entire cell body, see indeed Figs. 4(A, bottom panel) and 5. Finally, the enhancement in nucleus elasticity results in a significant change in the migratory phenotype of the cells in the smallest channel, as now half of them can invade the structure. This change in the motile behavior is the obvious consequence of the fact that cells are now able to compress and pull their nuclear region within the confined environment, as represented in Fig. 4(A, bottom panel) and (C). The different phenotypes of deformable cells within either the intermediate or the smallest channel are clearly captured in Fig. 6, where we compare the time development of their distribution along the two structures. At $t = 2$ h, only the intermediate channel has been entered by a significant

number of individuals (i.e., this is also a measure of a lower entry time, see Fig. 5(top panel)). Indeed, at the end of the observation time (i.e., at $t = 8$ h), most cells in the middle structure have reached the opposite border, whereas the total amount of individuals migrating in the subnuclear structure still localize in the central part of the device.

The computational findings are supported by a number of experimental approaches. In [3], glioma cell lines have been shown to squeeze through narrow locations in a brain model *in vivo*, thereby increasing their metastatic potential, by significantly compressing their nucleus upon recruitment of nonmuscle myosin II (NMMII). Moreover, very recently, other authors have been provided that the directional persistence of cancer cells in microsized structures is mainly regulated by the steric hindrance due to the presence of a rigid and voluminous nucleus [28, 29]. In particular, in [4, 53], Panc-1 cells have been shown to overcome size exclusion in microchannels architectures upon treatments with bioactive SPC. Finally, in [37], the authors have demonstrated that the number of acute promyelocytic leukemia (APL) cells able to migrate through filters of 5 μm (i.e., smaller than cell diameters) significantly reduced upon exposition to paclitaxel, which stabilizes the intracellular microtubule network. Analogous results have been provided therein also with primary human neutrophils moving in 3 μm-size pores.

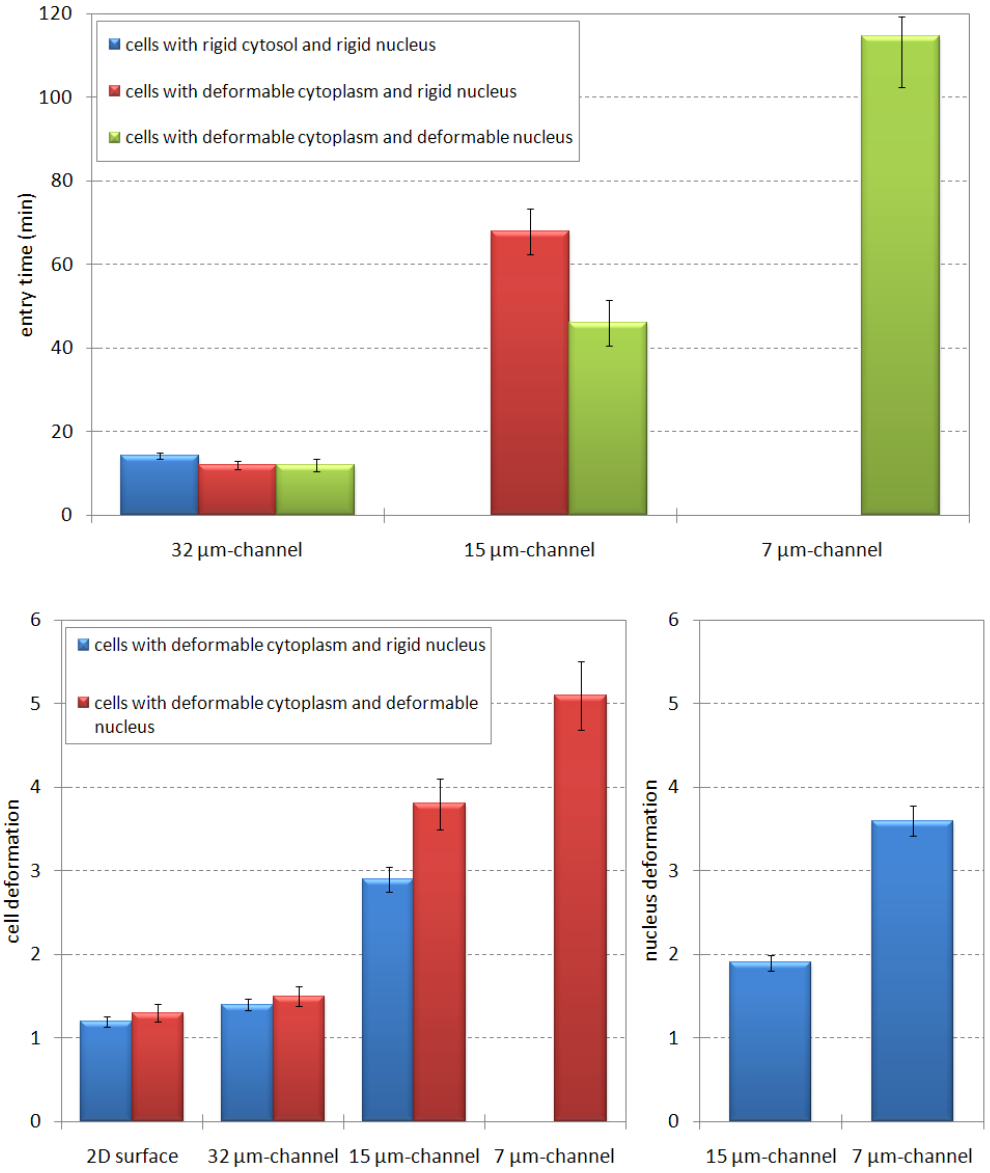

Figure 5: Top plot: comparison of the entry time of cells moving within the different microchannels. The entry time in the larger channel is substantially low, and does not significantly depend on the elastic properties of intracellular compartments. On the contrary, in the intermediate channel, the entry time significantly decreases upon the enhancement of the nucleus deformability. Finally, in the subnuclear structure, the entry time increases again because the nucleus, which is however stiffer than the cytosolic region, has to completely squeeze and elongate. Bottom plots: cell and nucleus deformation in the different structures. On both the bidimensional substrate and within the larger channel, cells do not need to deform, whereas they strongly remodel in more confined structures. In particular, in the intermediate channel, the nucleus elasticity further enhances cell shape reorganizations. In the subnuclear environment, the nucleus deforms even more dramatically to allow the whole individual to invade the channel. The deformation of rigid cells (respectively, of rigid nuclei) is obviously equal to 1 as the initial and final values of the cell (respectively, of nucleus) surface are the same. All the values in the plots are represented as means $\pm$ s.d. over 50 "effective" realizations. This means that, for this statistical analysis, we only consider cells that completely enter within the channel of interest (i.e., with an invasive or permeative phenotype). The others are classified as non-motile, assigned undefined entry time and deformation, and do not taken into account. Finally, if in a given case the number of cells entering a channel structure is not significant, we do not evaluate the relative quantity of interest. In particular, statistical significance ($p < 0.05$) is determined via both the Students' t-test for motile fraction data and via the Kolmogorov-Smirnov test for non-normally distributed data sets. The specific values regulating the elastic properties of the cell subcompartments are those used in the relative sets of simulations and explicitly cited in the text.

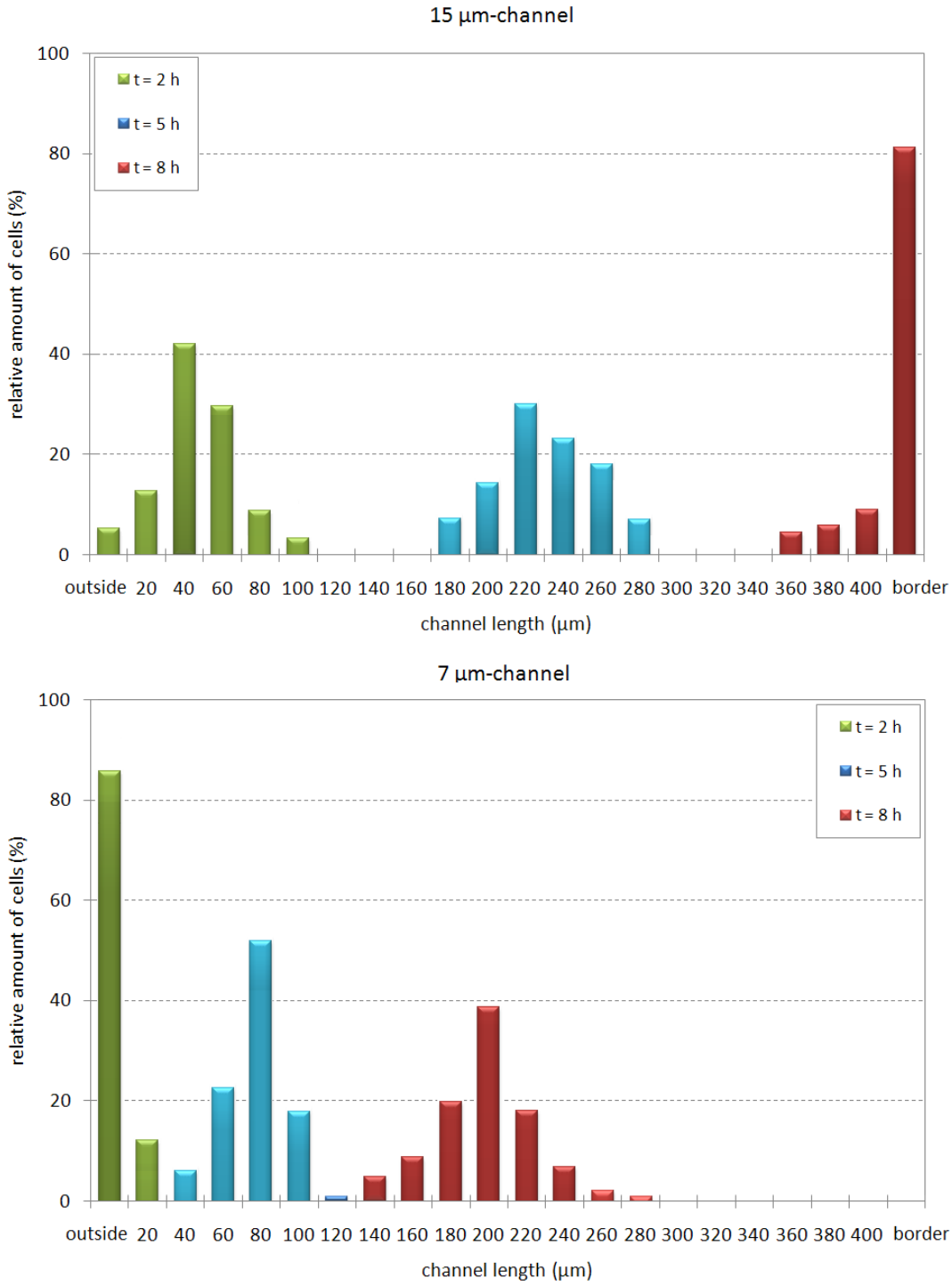

Figure 6: Time development of the cell distribution along the intermediate and small channels in the case of individuals with an elastic nucleus and a deformable cytoplasm. The permeative behavior of cells within the middle structure is clearly reproduced, as at 8 hours most of them have reached the border of the device. On the contrary, cells within the subnuclear structure are still in the middle of the channel, i.e., displaying a typical invasive phenotype. The entry time characterizing each channel, plotted in Fig. 5, is here pointed out from the fact that at 2 hours only the intermediate channel has been entered by a significant number of individuals. The values represented in the histogram plot are obtained by performing 100 ”effective” simulations, i.e., by taking into account only cells that completely enter within the channel of interest (see definition in Fig. 5).

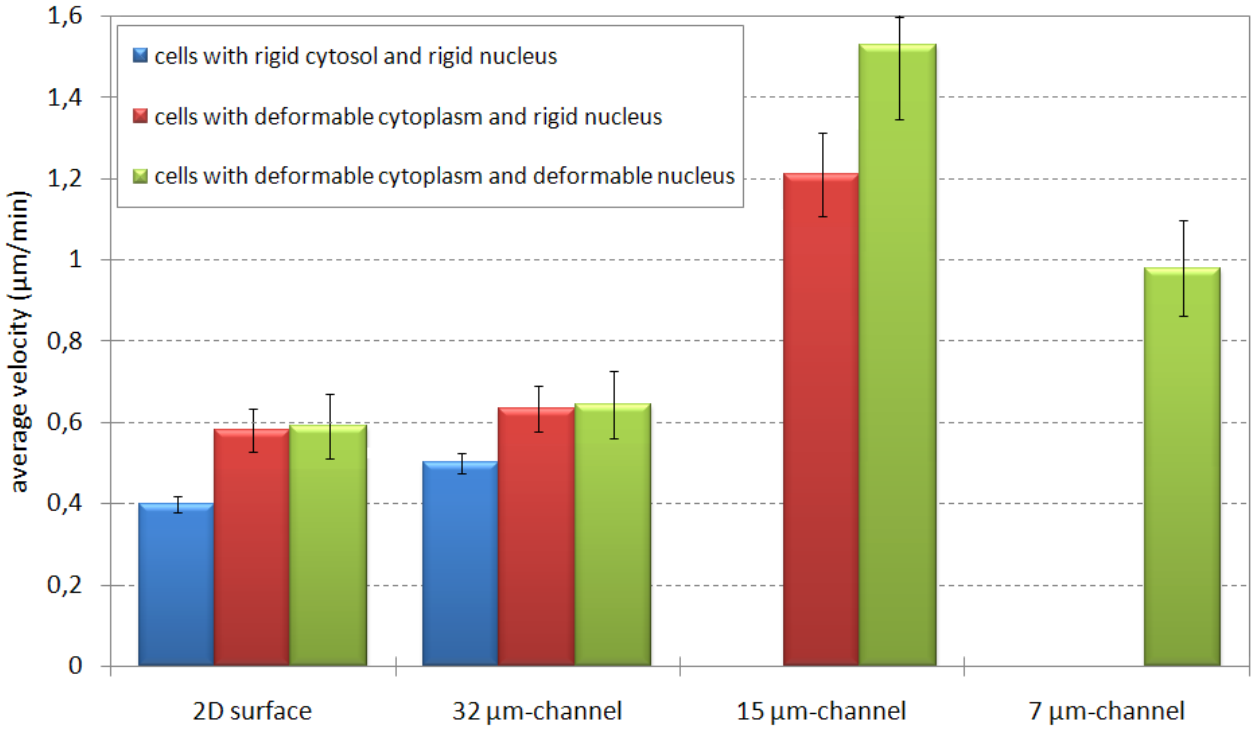

Figure 7: Comparison of the average migration speed of cells moving either on the flat surface or within the different microchannels. Cell velocity on both the bidimensional substrate and in the larger channel is substantially low, and does not significantly depend on the cytosol and nucleus rigidities. On the contrary, cell speed within the more confined structures is generally two-fold higher and is further enhanced by the possibility of nucleus deformability. The values of the cell average velocity are represented as means $\pm$ s.d. over 50 "effective" (see definition in Fig. 5) realizations.

Migration Velocities

In Fig. 7, we analyze the average velocity of cells, defined as the average velocity of their center of mass [42, 46, 57], both on the flat surface and within the different channel structures. This comparison allows to elucidate and to further quantify the differences between cell migratory phenotypes in specific geometric conditions. The random movement of rigid cells on the planar substrate is characterized by a low 0.4 μm/min-speed, which slightly increases for individuals with a deformable cytoplasm, reaching almost 0.6 μm/min. Indeed, there is no further variation upon the enhancement of the nuclear compressibility. An analogous behavior, with almost similar values, is observed for cell migration in the largest channel, confirming that extracellular environments whose dimensions are greater than cellular measures do not represent guidance cues, but rather behave as open spaces. In the case of the intermediate channel, cells with an elastic cytosol display instead an approximately two-fold increment in cell migration speed ($\approx$ 1.1 μm/min), which is significantly enhanced when allowing nuclear deformability ($\approx$ 1.5 μm/min). The different migration speeds of cells within either the big or the middle structure indeed reflect the different overall phenotypes, i.e. invasive and

permeative, respectively. Finally, in the case of the smallest channel, the cell average velocity (obviously evaluated only for cells with an elastic nucleus) slightly decreases again to less than 1 μm/min. The explanation resides in the fact that although the nucleus is deformable, it is however stiffer (and less motile) than the surrounding cytoplasm and therefore takes more time to remodel and move, slowering the overall individual, as also captured in Fig. 6, where the rate of advance of cells within the subnuclear structure is much more slower than that in the intermediate channel, and described below more in details.

These results first reveal two distinct migratory phenotypes, that are proposed to occur for cells placed either in open structures (i.e., 2D surfaces or large channels) or in confined architectures (i.e., channels smaller than cellular dimensions). In the first case, the movement of cells is widely independent from their elastic properties, whereas it is widely known to strongly rely on their adhesive strengths [34]. On the contrary, the efficacy of cell migration in 3D constrained environments is mainly determined by the deformation ability of the moving individuals (in particular, of their voluminous nucleus), which adapt to the geometrical characteristic of the environment. At this regard, it is indeed possible to identify an optimal dimension of an extracellular structure which results in a sustained cell locomotion: smaller than the cellular measures but higher than the nuclear diameter.

The drastic differences in cell migration speeds due to the specific environment dimensionality, captured by the model, are consistent with recent studies performed on NIH-3T3 fibroblasts [7], leukocytes [34] and pancreatic cancer cells [53]. In these cases, the authors have in fact demonstrated that cell movement in 3D confined structures is more rapid, uniaxial and closely dependent on cell morphological transitions. In striking contrast, the basic program of cell migration over flat ECM substrates strongly requires a dynamical adhesion to their environment via adhesive molecules, i.e. integrins, which generate the force necessary for propulsion and movement [1, 36]. Analogous conclusions have been found also by a theoretical model, which has reported that the migration of cells in a microsized channel strongly depends on partial pressure differences formed between the channel walls and either the leading or the rear edge of the individual, without the necessity of specific cell-surface adhesion molecules [24].

Migration Modes

We finally investigate whether in the different cases cells display a specific phenomenological/mechanical movement. In particular, in order to elucidate if cell distinct parts show coordinated movement, we separately track the leading edge, the nucleus and the rear edge of the cells, and we plot their absolute position inside a channel vs time in a 2-h span. Indeed, we consider the case of completely deformable individuals (i.e., with elastic subcompartments). As reproduced in Fig. 8 (top and middle panels), for large and medium channels, we observe a smooth *sliding* motion, characterized by an equidistant movement of the cell internal regions, which maintain the overall cell length. In

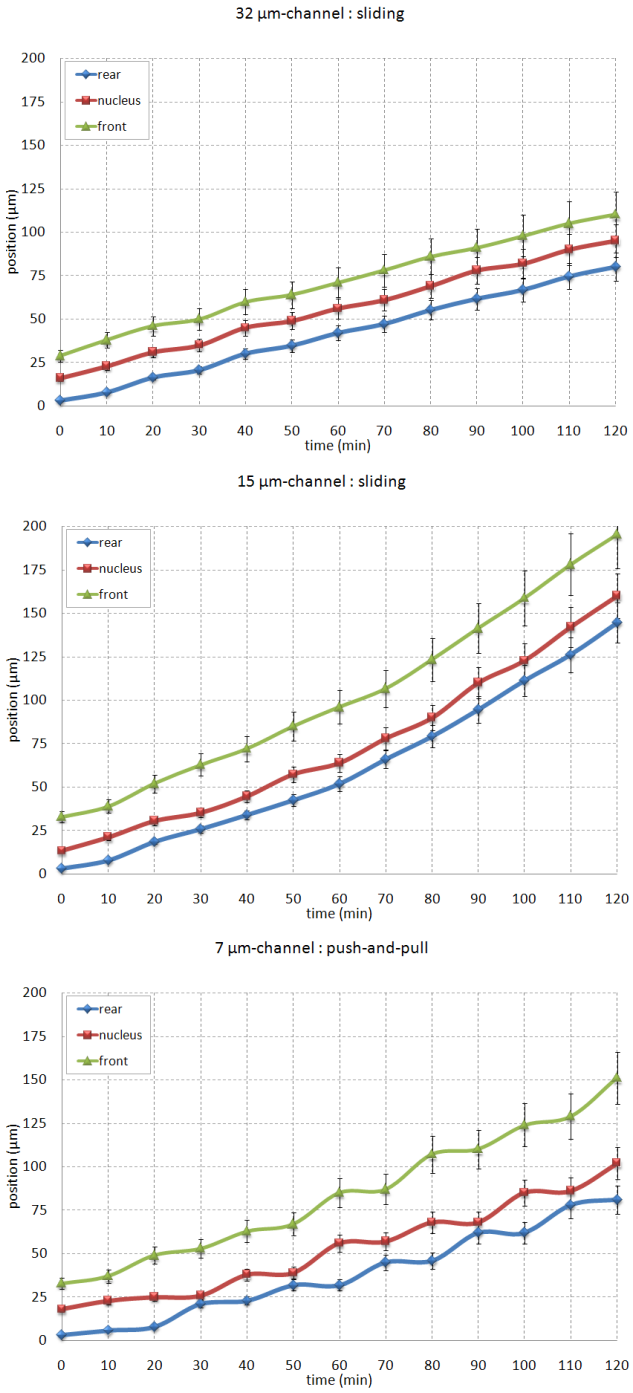

Figure 8: Cell migration dynamics inside the different channels in the case of cells able to remodel both their cytoplasm and their nucleus. Typical profile of a sliding-like migration pattern, where the cell front, nucleus and rear are moving in a synchronous way, is observed for large and intermediate channel structures (top and middle panels). Typical profile of a push-and-pull-like migration behavior, where the cell front smoothly moves while rear moves in an oscillating manner (i.e., depending of the time taken by nucleus to deform and displace) is found in the case of the smallest channel (bottom panel). The relative position of the different cell parts is plotted as the mean $\pm$ s.d. over 50 "effective" (see definition in Fig. 7) realizations.

particular, in the intermediate structure, cell front is significantly distant from the central and the back parts of the individual: this is due to the elongation process (captured also in Fig. 8) caused by the confined geometry of the channel. On the contrary, in the smallest channel, cells display a step-wise *push-and-pull* behavior, characterized by oscillating variations of cell length, see Fig. 8 (bottom panel), which has been also observed in [53]. This migratory phenomenology has a possible interesting mechanical explanation. The geometry of the channel in fact causes the cytosolic front of the cell to protrude. Pushed by the leading front, the overall cytosolic region, characterized by high elasticity and mobility, then deforms and moves forward, while pulling onto the nucleus with the force exerted through the contact tension $J^{int}_{N,C}$. However, as a consequence of its lower elasticity and motility (i.e., $T_N < T_C$ and $\nu_N > \nu_C$), the nuclear cluster takes more time to remodel toward a very elongated morphology and to displace and therefore lags behind (as reproduced in Fig. 4 and explained in more details for the chemotactic migration of an endothelial cell in [57]), limiting the elongation of the overall cell (which has to maintain its volume). Indeed, the displacement of the trailing part of the cytosol decreases the length of the individual. However, when such a rear part has moved far enough to the right, the nucleus, in order to avoid the split of the cell, is forced to move. Therefore it pushes the leading part of the cell, which can go on elongating, increasing again the overall cell length. It is useful to notice that this dramatic and continuous reorganization of the nuclear cluster is not necessary for cell movement in middle and large channels. Indeed, in those cases, the nucleus undergoes only slightly deformations and is therefore more easily dragged by the rest of the cell, whose whole locomotion is eventually characterized by the above-described sliding dynamics.

The push-and-pull pattern is similar to the classical migration of fibroblasts on flats surfaces [36], and is consistent with the results obtained again in [53] for pancreatic cancer cells moving in microchannel structures.

Invasion in a Fiber Structure

The analysis of the results provided in the previous sections suggests that the elastic properties of the nucleus strongly determine the motile behavior of the overall cell in confined architectures. In particular, cells fail to neck down to micrometer dimensions and, for instance, to migrate through steric barriers with pore size smaller than nuclear diameter when their nucleus is stiff. Even in the case of elastic nuclei, it is then expected that invasion is hampered by an exceedingly small pore size. However, as explained in the Introduction, cancer cells typically move within fibrous extracellular matrices, whose topological structure locally changes, so that they have to constantly adapt their morphology.

In order to check how such specific environments affect cell locomotion, we employ the proposed model to consider cell motion in isotropic 3D scaffolds, formed by regular cubic meshes with varying pore size, see Fig. 9(A). In this case, the simulation domain $\Omega \subset \mathbb{R}^3$ is a $120 \times 120 \times 120$ regular grid, with periodic boundary conditions in

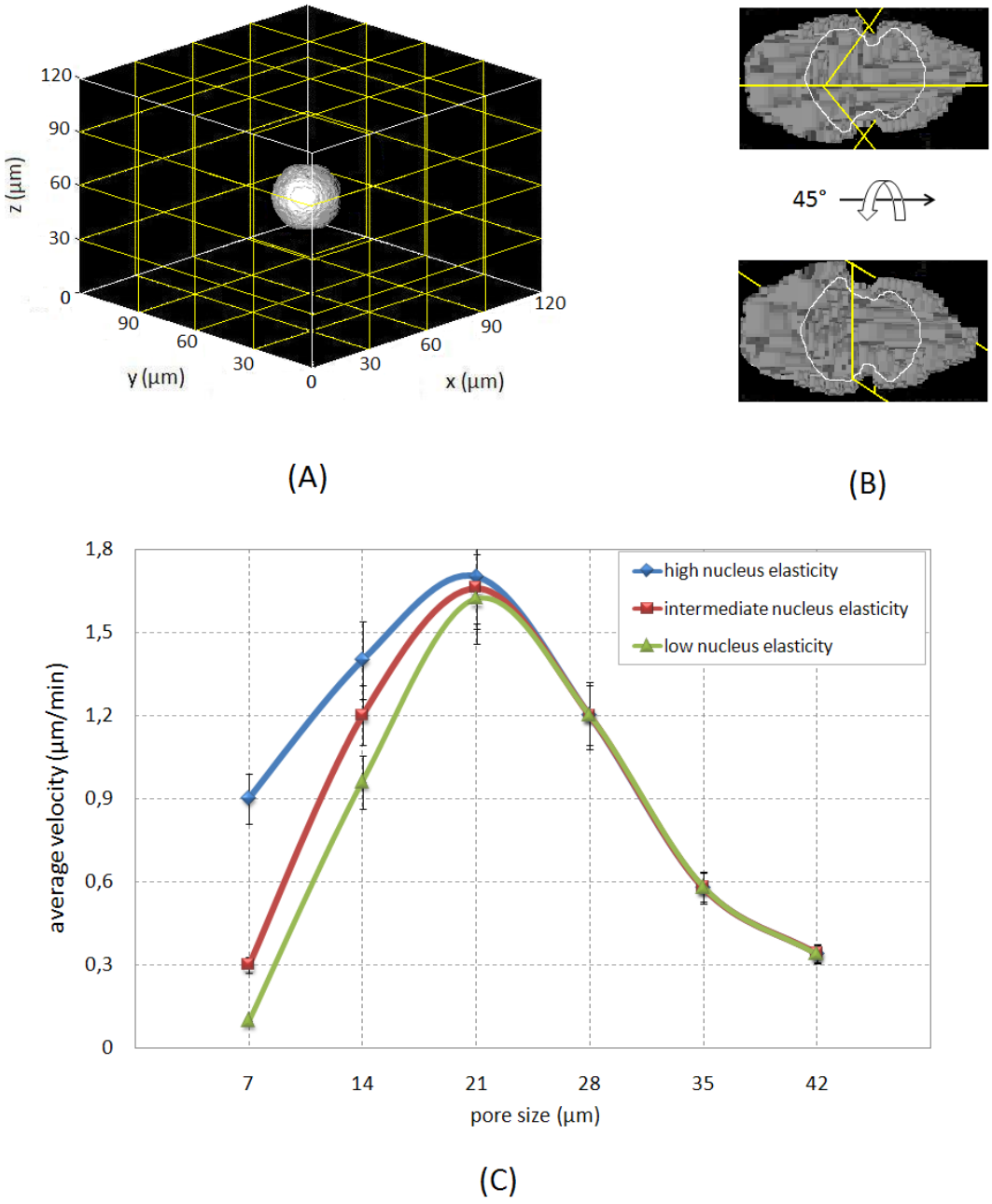

Figure 9: Cell invasion within a 3D network structure, resembling an *in vivo* fibrous matrix. (A) Simulation domain Ω, containing both an isotropic cubic mesh of collagenous threads (yellow stripes) and the interstitial medium (black). For representative purposes, we depict a scaffold with a uniform distribution of pores of 30 μm side length. (B) Magnifications from different angles of a moving cell in the case of pores smaller than nucleus diameters (i.e., 7 μm). For better visualization, the nucleus is encircled manually. It is straightforward to see how the nucleus has to squeeze to allow the entire individual to pass though the fiber network. (C) Velocity vs pore size in the case of cells with different nucleus elasticities: $\nu_N = 15$ (low elasticity, green line); $\nu_N = 8$ (intermediate elasticity, red line); $\nu_N = 0.9$ (high elasticity, blue line). The values are represented as means $\pm$ s.d. over 50 realizations.

all directions. The characteristic size of each grid site (1 μm), as well as the overall observation time (8 hours), is the same as in the simulations presented in the previous sections. In the center of the domain, we seed an individual cancer cell, which is initially a sphere whose volume, as the dimension of its nucleus, remains unaltered from Sec. 3.1. The cell moves following the *hamiltonian* defined in Eq. (2). In particular, we assume that the cell cytosol is deformable (by a low $\nu_C = 0.5$), whereas we vary the elasticity of the nuclear compartment.

In all cases, the cell displays a random walk through matrix pores, without preferred direction: given the isotropy of the scaffold, the persistent term (5) in fact does not significantly affect cell movement. However, its velocity is specifically determined by the correlation between the elastic properties of its nucleus and the density of the scaffold. As shown in Fig. 9(C), at high pore sizes (i.e., in the same range of cell diameter), cell migratory behavior remains unaltered regardless of the deformation abilities of the nuclear compartment. In fact, the moving individual does not sense significative steric hindrances, since the distance from the nearest matrix fiber is too high to experience any interaction and, in all cases, it exhibits a short-range movement with fluctuations in the interstitial medium around its initial position.

The formation of pore diameters of cellular or slightly subcellular ranges (say (14 μm ; 28 μm)) allows instead the cell to physically interact with fibers in all three spatial directions and is associated with the most efficient migration rates. In this case, migrating cell assumes an elongated morphology and slightly reduce its diameters to pass through the matrix network. In particular, nuclear elasticity provides a further facilitation for cell movement (i.e., the speed slightly increases), since it allows moving individual to more easily squeeze and stretch through the existing mesh. This results is indeed consistent with the motile behavior of cells within the intermediate channel presented so far.

Finally, an increase in the abundance of 3D matrix threads results in a scaffold characterized by small pores (< 10 μm, i.e. smaller than nuclear size) with limited available space. Indeed, only the cell with a softest nucleus display an appreciable migration speed, which is not achieved in the other cases. For a cell characterized by a stiffer nucleus, even the formation of long cytosolic protrusions is in fact not sufficient to pass through such steric hindrances, since the nucleus can not significantly deform, which causes the overall individual to be confined in a small area, see the representative phenomenology in Fig. 9(B). Analogous observations have previously emerged for cells moving in the subnuclear channels.

The bimodal behavior of cell speed in response to pore dimensions predicted by our simulations is similar to those presented in a number of experimental works, such as for human adult vascular smooth muscle cells (HSMCs) seeded in type IV collagen (CnIV) scaffolds [6] or human glioma cells plated on polyacrylamide ECMs [63], and for different fibroblastic and cancerous cell lines migrating within 3D fibrous matrices of similar geometrical and structural properties, i.e., NR6 mouse fibroblasts in collagen-glycosaminoglycan matrices [23], or human melanoma

cells in collagen lattices [11]. Moreover, neutrophil migration (both velocity and directional coefficient) has been reported to vary in a biphasic manner with the gel pore size [32], while mouse fibroblasts have been observed to migrate more significantly in collagen-glycosaminoglycan (CG) scaffolds featuring pore sizes somewhat smaller than cellular dimensions, whereas they have exhibited less dispersion in matrices with larger pores [23].

Discussion

Due to the increasingly recognized importance of cell migration processes in confined matrix environments, and their exploitation for therapy and tissue engineering, a number of experimental models has been recently developed. Most of them focus on giving insight into selected adhesive and proteolytic mechanisms, which have typically represented the preferential targets for treatment strategies in cell migration-associated disorders and cancer development. However, an increasing amount of evidence has recently shown that pivotal regulators of cell movements, and therefore potential targets for pharmacological interventions in human diseases, are also the elastic properties of intracellular subcompartments, i.e., the cytoskeleton and the nucleus. New perspectives on this issue have been developed by experimental assays that consist either of migration chips characterized by channel structures of various dimensions or of fibrous scaffolds, which feature pores of specific sizes. Indeed, in the last few years, these single-cell based approaches have provided efficacy to study and unraveling the migratory and invasive behavior of different normal and tumor cell lines, as provided in [11, 23, 28, 29, 53, 66] and references therein.

In this work, we have employed a simple and intuitive version of the Cellular Potts Model to reproduce cell migration both in microchannels and within fibrous networks. The CPM used here is able to treat cancer cells as compartmentalized physical objects, differentiated into nucleus and cytoplasm, which resulted to be a fundamental aspect in describing cell motile behavior in structures with subcellular dimensions. It in fact allowed to describe the specific mechanical/elastic properties of each intracellular compartment, and to analyze their distinct influence on cell migratory phenotype.

For instance, we have provided evidence that the migratory behavior of cancer cells within channels larger than their dimensions is widely independent from their deformation ability, as moving individuals maintain a common invasive phenotype. In narrower 3D structures, cells have instead to overcome the effects of size exclusion. Indeed, they can move within intermediate channels, acquiring a permeative behavior, by reorganizing and squeezing their cysoskeletal region. Eventually, only an induced softening, and the subsequent compression, of the voluminous nucleus enables moving cells to invade subnuclear architectures.

The proposed simulated migration chip has also allowed a quantification of the drastic differences in cell migration

speeds, which strongly rely on the specific dimensionality of the environment, as also provided by recent experimental studies [7, 49, 53]. In particular, cell speed on both 2D flat surfaces and within large 3D structures has been provided to be slightly influenced by variations in the elastic properties of cell cytosol, whereas it is completely un-affected by the mechanical characteristics of the nuclear cluster. This is consistent with the experimental observation that the predominant mechanisms underlying cell movement in open spaces mainly depend on adhesive interactions and not on geometrical considerations, as steric hindrances have only a minor influence [7, 34]. On the contrary, cell migratory ability in more constrained structures significantly depends and is enhanced by the elastic/mechanical deformations of both intracellular compartments.

At this regard, we have finally speculated about a transition between two distinct motile dynamics: a smooth sliding movement, which maintains cell length and characterizes cell locomotion within architectures larger than nucleus dimensions, and a push-and-pull movement, observed in the subnuclear channel. In particular, this second migratory phenotype is the result of the time taken by the nuclear cluster to remodel, squeeze and displace.

Applying the model for the study of cell motion in a fibrous matrix, we have provided evidence that cell maximal dispersion occurs at intermediate thread densities, i.e. within scaffolds with a fiber mesh of an optimal size for a cell to squeeze through. Indeed, if the inter-fiber distance becomes too wide, moving cells loose the availability of anchorage points and the contact guidance necessary for traction and further movement. On the contrary, if the fiber network is formed by small pores, a significant cell movement can only be achieved through a dramatic contractility of its nucleus.

In all the proposed cases, the computational results have been consistent with a number of published experimental counterparts, representing further complementary determinations. In particular, our study may contribute to a more detailed understanding of how cancer cells invade surrounding confined tissues, escaping from a primary tumor and permeating through the stroma (which is the first step in tumor spreading). Our simulated migration assays may indeed provide an easy system to promote current research on 3D migration behavior at the single-cell level. As a clear advantage of a theoretical approach, it in fact allows to independently vary and modulate in a graded fashion all cell biophysical parameters and selected microstructural properties of the matrix environment, which is helpful in dissecting the complex relationships between cell motility and the specific geometrical properties of the environment. At this regard, it would be biologically relevant to adapt our approach to specific tumor cell lines, characterized by distinct biophysical phenotypes (i.e., intrinsic motility or elasticity). This can be easily done by inheriting the model parameters from experimentally-measured quantities, characteristic of the selected cell population. It would be also interesting to analyze collective migrations of cellular ensembles, which are fundamental in several pathological processes, as commented in [27]. A differentiation may in fact occur among individuals of the same family, such as tip

and stalk cells during tumor-induced angiogenic processes, or leader and follower cells during tumor front invasions [16].

However, the present modeling approach is unable to encompass some mechanisms underlying cell migration in confined structures. Some of these additional, here disregarded, factors are (i) the role played by local pressure differences between the cell membrane and the channels walls (which has been described in detail in [24]); (ii) the molecular activity of cell motor units, with the driving actin-polymerization (i.e., lamellipodial extension) in the front of the individual and the contractive acto-myosin assembly at its rear; (iii) the inside-out mechanical signals (i.e., shear stress) transmitted from the external environment to the cells, thereby changing the activity of specific proteins mediating cell locomotion (such as Rac, Rho) [12].

References

[1] Alberts, B., Bray, D., Lewis, J., Raff, M., Roberts, K., Watson J. D., 1994. *Molecular Biology of the Cell, 3rd edition.* Garland Science.

[2] Balter, A., Merks, R., M., H., Poplawski, N., J., Swat, M., Glazier, J., A., 2007. *The Glazier-Graner-Hogeweg model: extensions, future directions, and opportunities for further study.* In A. R. A. Anderson, M. A. J. Chaplain, and K. A. Rejniak editors, *Single-Cell-Based Models in Biology and Medicine*, Mathematics and Biosciences in Interactions, Birkaüser, 151 - 167.

[3] Beadle, C., Assanah, M. C., Monzo, P., Vallee, R., Rosenfeld, S. S., Canoll, P., 2008. *The role of myosin ii in glioma invasion of the brain.* Mol Biol Cell, 19, 3357 - 3368.

[4] Beil, M., Micoulet, A., Wichert, G., Paschke, S., Walther, P., et al., 2003. *Sphingosylphosphorylcholine regulates keratin network architecture and viscoelastic properties of human cancer cells.* Nat Cell Biol, 5, 803 - 811.

[5] Chen, J., Irianto, J., Inamdar, S., Pravincumar, P., Lee, D. A., Bader, D. L., Knight, M. M., 2012. *Cell mechanics, structure, and function are regulated by the stiffness of the three-dimensional microenvironment.* Biophys J, 103 (6), 1188 – 1197.

[6] DiMilla, P. A., Stone, J. A., Quinn, J. A., Albelda, S. M., Lauffenburger, D. A., 1993. *Maximal migration of human smooth-muscle cells on fibronectin and type-IV collagen occurs at an intermediate attachment strength.* J Cell Biol, 122, 729 - 737.

[7] Doyle, A. D., Wang, F. W., Matsumoto, K., Yamada, K. M., 2009. *One-dimensional topography underlies three-dimensional fibrillar cell migration.* J Cell Biol, 184, 481 - 490.

[8] Egeblad, M., Rasch, M. G., Weaver, V. M., 2010. *Dynamic interplay between the collagen scaffold and tumor evolution.* Curr. Opin Cell Biol, 22, 697 - 706.

[9] Erler, J. T., Weaver, V. M., 2009. *Three-dimensional context regulation of metastasis.* Clin. Exp. Metastasis, 26, 35 - 49.

[10] Friedl, P., Brocker, E. B., 2000. *The biology of cell locomotion within three-dimensional extracellular matrix.* Cell Mol Life Sci, 57 (1), 41 - 64.

[11] Friedl, P., Maaser, K., Klein, C. E., Niggemann, B., Krohne, G., Zänker, K.S.,1997. *Migration of highly aggressive MV3 melanoma cells in 3-dimensional collagen lattices results in local matrix reorganization and shedding of alpha2 and beta1 integrins and CD44*. Cancer Res, 57 (10), 2061 – 2070.

[12] Friedl, P., Wolf, K. 2003. *Tumour-cell invasion and migration: diversity and escape mechanisms.* Nat Rev Cancer, 3 (5), 362 - 374.

[13] Friedl, P., Wolf, K., 2010. *Plasticity of cell migration: a multiscale tuning model* J Cell Biol, 188, 11 - 19

[14] Friedl, P., Wolf, K., Lammerding, J., 2011. *Nuclear mechanics during cell migration.* Curr Opin Cell Biol, 23 (2), 253.

[15] Friedl, P., Weigelin, B., 2008. *Interstitial leukocyte migration and immune function.* Nat Immunol. 9 (9), 960 - 969.

[16] Friedl, P., Gilmour, D., 2009. *Collective cell migration in morphogenesis, regeneration and cancer.* Nat Rev Mol Cell Biol, 10, 445 – 457.

[17] Gerlitz, G., Bustin, M., 2011. *The role of chromatin structure in cell migration.* Trends Cell Biol, 21 (1), 6 – 11.

[18] Glazier, J. A., Balter, A., Poplawski, N. J., 2007. *Magnetization to morphogenesis: A brief history of the Glazier-Graner-Hogeweg model.* In A. R. A. Anderson, M. A. J. Chaplain, and K. A. Rejniak editors, *Single-Cell-Based Models in Biology and Medicine*, Mathematics and Biosciences in Interactions, Birkaüser, 79 - 106.

[19] Glazier, J. A., Graner, F., 1993. *Simulation of the differential adhesion driven rearrangement of biological cells*. Physical Rev E, 47, 2128 - 2154.

[20] Graner, F., Glazier, J. A., 1992. *Simulation of biological cell sorting using a two dimensional extended Potts model.* Phys Rev Lett, 69, 2013 - 2017.

[21] Guck, J., Lautenschläger, F., Paschke, S., Beil, M., 2010. *Critical review: Cellular mechanobiology and amoeboid migration.* Integr Biol, 2 (11), 575 583.

[22] Guck, J., Schinkinger, S., Lincoln, B., Wottawah, F., Ebert, S., Romeyke, M., Lenz, D., Erickson, H. M., Ananthakrishnan, R., Mitchell, D., Ks, J., Ulvick, S., Bilby, C., 2005. *Optical deformability as an inherent cell marker for testing malignant transformation and metastatic competence.* Biophys J, 88 (5), 3689 – 3698.

[23] Harley, B. A. C., Kim, H., Zaman, M. H., Yannas, I. V., Lauffenburger, D. A., Gibson, L. J., 2008. *Microarchitecture of three-dimensional scaffolds influences cell migration behavior via junction interactions.* Biophys J, 95 (8), 4013- 4024.

[24] Hawkins, R., Piel, M., Faure-Andre, G., Lennon-Dumenil, A., Joanny, J., et al., 2009. *Pushing off the walls: a mechanism of cell motility in confinement.* Phys Rev Lett, 102, 4.

[25] Hotary, K. B., Allen, E. D., Brooks, P. C., Datta, N. S., Long, M. W., Weiss, S. J., 2003. *Membrane type I matrix metalloproteinase usurps tumor growth control imposed by the three-dimensional extracellular matrix.* Cell, 114, 33 - 45.

[26] Huang, S., Brangwynne, C. P., Parker, K. K., Ingber, D. E., 2005. *Symmetry-breaking in mammalian cell cohort migration during tissue pattern formation: role of random-walk persistence.* Cell Motil Cytoskeleton, 61 (4), 201 - 213.

[27] Ilina, O., Bakker, G. J., Vasaturo, A., Hofmann, R. M., Friedl, P., 2011. *Two-photon laser-generated microtracks in 3D collagen lattices: principles of MMP-dependent and -independent collective cancer cell invasion.* Phys Biol, 8 (1), 015010.

[28] Irimia, D., Charras, G., Agrawal, N., Mitchison, T., Toner, M., 2007. *Polar stimulation and constrained cell migration in microfluidic channels.* Lab on a Chip, 7, 1783.

[29] Irimia, D., Toner, M., 2009. *Spontaneous migration of cancer cells under conditions of mechanical confinement.* Integr Biol, 1, 506 - 512.

[30] Ising, E., 1925. *Beitrag zur theorie des ferromagnetismus.* Z Physik, 31, 253.

[31] Kumar. S., Weaver, V. M., 2009. *Mechanics, malignancy, and metastasis: The force journey of a tumor cell.* Cancer and Metastasis Reviews, 28, 113 - 127.

[32] Kuntz, R. M., Saltzman, W. M., 1997. *Neutrophil motility in extracellular matrix gels: mesh size and adhesion affect speed of migration.* Biophys J, 72 (3), 1472 - 1480.

[33] Kurosaka, S., Kashina, A., 2008. *Cell biology of embryonic migration.* Birth Defects Res C Embryo Today, 84 (2), 102 - 122.

[34] Lämmermann, T., Bader, B. L., Monkley, S. J., Worbs, T., Wedlich-Soldner, R., et al., 2008. *Rapid leukocyte migration by integrin-independent flowing and squeezing.* Nature, 453, 51 - 55.

[35] Lauffenburger, D. A., Lindermann, J. J., 1996. *Receptors: Models for Binding, Trafficking, and Signaling.* Oxford University Press, London.

[36] Lauffenburger, D. A., Horwitz, A. F., 1996. *Cell migration: a physically integrated molecular process.* Cell, 84 (3), 359 - 369.

[37] Lautenschläger, F., Paschke, S., Schinkinger, S., Bruel, A., Beil, M., Guck J., 2009. *The regulatory role of cell mechanics for migration of differentiating myeloid cells* Proc Natl Acad Sci U. S. A., 106 (37), 15696 – 15701.

[38] Lee, C. H., Kim, M. S., Chung, B. M., Leahy, D. J., Coulombe, P. A., 2012. *Structural basis for heteromeric assembly and perinuclear organization of keratin filaments.* Nat Struct Mol Biol, 19 (7), 707 – 15.

[39] Luger, K., Dechassa, M. L., Tremethick, D. J., 2012. *New insights into nucleosome and chromatin structure: an ordered state or a disordered affair?* Nat Rev Mol Cell Biol, 13 (7), 436 – 447.

[40] Marée, A., F., M., Grieneisen, V., A., Hogeweg, P., 2007. *The Cellular Potts Model and biophysical properties of cells, tissues and morphogenesis*. In A. R. A. Anderson, M. A. J. Chaplain, and K. A. Rejniak editors, *Single-Cell-Based Models in Biology and Medicine* , Mathematics and Biosciences in Interactions, Birkaüser, 107 - 136.

[41] Merks, R. M. H., Glazier, J. A., Brodsky, S. V., Goligorksy, M. S., Newman, S. A., 2006. *Cell elongation is key to in silico replication of in vitro vasculogenesis and subsequent remodeling.* Develop Biol, 289, 44 - 54.

[42] Merks, R. M. H., Perryn, E. D., Shirinifard, A., Glazier, J. A., 2008. *Contact-inhibited chemotactic motility: role in de novo and sprouting blood vessel growth.* PLOS Comp Biol, 4, e1000163.

[43] Metropolis, N., Rosenbluth, A. E., Rosenbluth, M. N., Teller, A. H., Teller, E., 1953. *Equation of state calculations by fast computing machines.* J Chem Phys, 21, 1087 - 1092.

[44] Mogilner, A., Oster, G., 2003. *Polymer motors: pushing out the front and pulling up the back.* Current Biology, 13 (18), R721 - R733.

[45] Pankova, K., Rosel, D., Novotny, M., Brabek, J., 2010. *The molecular mechanisms of transition between mesenchymal and amoeboid invasiveness in tumor cells.* Cell Mol Life Sci, 67 (1), 63 – 71.

[46] Perryn, E. D., Czirok, A., Little, C. D., 2008. *Vascular sprout formation entails tissue deformations and VE-cadherin dependent cell-autonomous motility.* Dev Biol, 313, 545 - 555.

[47] Pollard, T. D., Borisy, G. G., 2003. *Cellular motility driven by assembly and disassembly of actin filaments.* Cell, 112 (4), 453 - 465.

[48] Potts, R. B., 1952. *Some generalized order-disorder transformations.* Proc Camb Phil Soc, 48, 106 – 109.

[49] Pouthas, F., Girard, P., Lecaudey, V., Ly, T. B., Gilmour, D., et al., 2008. *In migrating cells, the Golgi complex and the position of the centrosome depend on geometrical constraints of the substratum.* J Cell Sci, 121, 2406 - 2414.

[50] Provenzano, P. P., Inman, D. R., Eliceiri, K. W., Knittel, J. G., Yan, L., Rueden, C. T., White, J. G., Keely, P. J., 2008. *Collagen density promotes mammary tumor initiation and progression.* BMC Med, 6 – 11.

[51] Remmerbach, T. W., Wottawah, F., Dietrich, J., Lincoln, B., Wittekind, C., Guck, J., 2009. *Oral cancer diagnosis by mechanical phenotyping.* Cancer Res, 69 (5), 1728 – 1732.

[52] Ridley, A. J., Schwartz, M. A., Burridge, K., Firtel, R. A., Ginsberg, M. H., Borisy, G., Parsons, J. T., Horwitz, A. R., 2003. *Cell migration: integrating signals from front to back.* Science, 302 (5651), 1704 - 1709.

[53] Rolli C. G., Seufferlein, T., Kemkemer, R., Spatz, J. P., 2010. *Impact of tumor cell cytoskeleton organization on invasiveness and migration: a microchannel-based approach.* PLoS ONE, 5, e8726. doi:10.1371/journal.pone.0008726

[54] Sahai, E., 2007. *Illuminating the metastatic process.* Nat Rev Cancer, 7 (10), 737 - 749.

[55] Schinkinger, S., Lincoln, B., Wottawah, F., Ebert, S., Romeyke, M., Lenz, D., Erickson, H. M., Ananthakrishnan, R., Mitchell, D., Ks, J., Ulvick, S., Bilby, C., 2005. *Optical deformability as an inherent cell marker for testing malignant transformation and metastatic competence.* Biophys J, 88, 3689 – 3698.

[56] Scianna, M., Merks, R. M. H., Preziosi, L., Medico, E., 2009. *Individual cell-based models of cell scatter of ARO and MLP-29 cells in response to hepatocyte growth factor.* J Theor Biol, 260 (1), 151 - 160.

[57] Scianna, M., 2011. *A multiscale hybrid model for pro-angiogenic calcium signals in a vascular endothelial cell.* Bull Math Biol, 74 (6), 1253 – 1291.

[58] Scianna, M., Preziosi, L., 2012. *Multiscale Developments of the Cellular Potts Model.* Multiscale Model Simul, 10 (2), 342 – 382.

[59] Scianna, M., Preziosi, L., Wolf, K., 2012. *A Cellular Potts Model simulating cell migration on and in matrix environments.* Submitted.

[60] Steinberg, M. S., 1963. *Reconstruction of tissues by dissociated cells. Some morphogenetic tissue movements and the sorting out of embryonic cells may have a common explanation.* Science, 141, 401 – 408.

[61] Steinberg, M. S., 1970. *Does differential adhesion govern self-assembly processes in histogenesis? Equilibrium configurations and the emergence of a hierarchy among populations of embryonic cells.* J Exp Zool, 173 (4), 395 – 433.

[62] Seufferlein, T., Rozengurt, E., 1995. *Sphingosylphosphorylcholine rapidly induces tyrosine phosphorylation of p125FAK and paxillin, rearrangement of the actin cytoskeleton and focal contact assembly. Requirement of p21rho in the signaling pathway.* J Biol Chem, 270, 24343 - 24351.

[63] Ulrich, T. A., De Juan Pardo, E. M., Kumar, S., 2009. *The mechanical rigidity of the extracellular matrix regulates the structure, motility, and proliferation of glioma cells.* Cancer Res, 69 (10), 4167 – 4174.

[64] Wyckoff, J. B., Jones, J. G., Condeelis, J. S., Segall, J. E., 2000. *A critical step in metastasis: in vivo analysis of intravasation at the primary tumor.* Cancer Res, 60 (9), 2504 – 2511.

[65] Wolf, K., Mazo, I., Leung, H., Engelke, K., von Andrian, U. H., Deryugina, E. I., Strongin, A. Y., Brocker, E. B., Friedl, P., 2003. *Compensation mechanism in tumor cell migration: mesenchymal-amoeboid transition after blocking of pericellular proteolysis.* J Cell Biol, 160, 267.

[66] Wolf, K., Wu, Y. I., Liu, Y., Geiger, J., Tam, E., et al., 2007. *Multi-step pericellular proteolysis controls the transition from individual to collective cancer cell invasion.* Nat Cell Biol, 9, 893 - 904.

[67] Wolf, K., Alexander, S., Schacht, V., Coussens, L. M., von Andrian, U. H., van Rheenen, J., Deryugina, E., Friedl, P., 2009. *Collagen-based cell migration models in vitro and in vivo.* Semin Cell Dev Biol, 20 (8), 931 – 941.

[68] Zaman, M. H., Matsudaira, P., Lauffenburger, D. A., 2007. *Understanding effects of matrix protease and matrix organization on directional persistence and translational speed in three-dimensional cell migration.* Ann Biomed Eng, 35 (1), 91 - 100.

[69] Zaman, M. H., Trapani, L. M., Sieminski, A. L., Mackellar, D., Gong, H., Kamm, R. D., Wells, A., Lauffenburger, D. A., Matsudaira, P., 2006. *Migration of tumor cells in 3D matrices is governed by matrix stiffness along with cell-matrix adhesion and proteolysis.* Proc Natl Acad Sci U. S. A., 103 (29), 10889 – 94.